LANGMUIR

pubs.acs.org/Langmuir Article

Repulsive Backbone–Backbone Interactions Modulate Access to Specific and Unspecific Binding Sites on Surface-Bound Mucins

Theresa M. Lutz, Matthias Marczynski, Maximilian J. Grill, Wolfgang A. Wall, and Oliver Lieleg*

Cite This: *Langmuir* 2020, 36, 12973–12982 Read Online

ACCESS | Metrics & More | Article Recommendations | Supporting Information

ABSTRACT: Mucin glycoproteins are the matrix-forming key components of mucus, the innate protective barrier protecting us from pathogenic attack. However, this barrier is constantly challenged by mucin-degrading enzymes, which tend to target anionic glycan chains such as sulfate groups and sialic acid residues. Here, we demonstrate that the efficiency of both unspecific and specific binding of small molecules to mucins is reduced when sulfate groups are enzymatically removed from mucins; this is unexpected because neither of the specific mucin-binding partners tested here targets these sulfate motifs on the mucin glycoprotein. Based on simulation results obtained from a numerical model of the mucin macromolecule, we propose that anionic motifs along the mucin chain establish intramolecular repulsion forces which maintain an elongated mucin conformation. In the absence of these repulsive forces, the mucin seems to adopt a more compacted structure, in which the accessibility of several binding sites is restricted. Our results contribute to a better understanding on how different glycans contribute to the broad spectrum of functions mucin glycoproteins have.

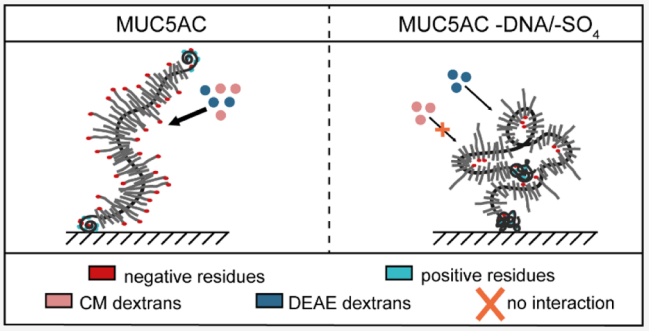

INTRODUCTION

With the current corona pandemic forcing most of the world's population to self-isolate, we are reminded that our innate immune system cannot fully protect us from all the pathogens the human body is exposed to. In healthy individuals, the first physical barrier invading pathogens encounter is the mucus layer that covers all wet epithelial tissues of the human body.[1−5] This hydrogel lining can retain microscopic objects such as dust particles[6,7] or bacteria[8,9] due to its mere size constraints. Additionally, mucin glycoproteins, which are the key component of mucus, can also immobilize small viruses—either *via* unspecific (hydrophobic or electrostatic) binding interactions or *via* specific binding to certain motifs of the mucin molecule such as sialic acid residues.[10−12]

This versatility of mucin-binding properties is based on the complex structure of the glycoprotein. Mucins are organized in three distinct sections: an elongated, hydrophilic, and highly glycosylated protein core is terminated by two hydrophobic, partially folded, and almost glycan-free termini. Despite their overall hydrophobic character, the mucin termini contain a large number of (both positively and negatively) charged amino acid side chains. The oligoglycan chains attached to the core of the polypeptide contain a large amount of sialic acid and sulfate groups, which convey an overall negative net charge to mucins—at least at neutral pH levels.[13−17]

In vivo, mucins are constantly challenged by enzymes, and those enzymes either originate from the mucin-secreting organisms[18,19] or from pathogens[20,21] which try to weaken the mucosal barrier. Indeed, anionic glycan motifs are a typical starting point for bacterial or viral degradation of mucins.[22] Previous work has already indicated how important the molecular integrity of mucins is for mucin functionality,[23,24] and also anionic mucin glycans have been put forward to be critical in this context[15] since the repulsive electrostatic forces acting between these anionic groups contribute to maintaining an elongated conformation. The weakening of intramolecular electrostatic repulsion is thought to result in a conformational change of this elongated bottle brush-like mucin structure into a rather globular state.[25−28] Such a severe conformational change can be expected to also affect the interaction of mucins with other particles, molecules,[29] or microorganisms[30] and thus the permeability of a mucin network toward these objects.

In this article, we show that the removal of anionic residues from porcine gastric mucin reduces the binding capability of mucin toward both cationic and anionic molecules as well as specific-binding partners, which do not directly target the anionic residues. By combining experimental data obtained from a molecular depletion assay, ELISA, and adsorption

Received: July 31, 2020
Revised: October 8, 2020
Published: October 22, 2020

https://dx.doi.org/10.1021/acs.langmuir.0c02256
Langmuir 2020, 36, 12973−12982

experiments with numerical simulations of mucins with different charge profiles, we propose that the mucin glycoprotein undergoes a conformational change when anionic glycans are removed. In turn, our results suggest that anionic residues along the mucin chain establish intramolecular repulsion forces that maintain the "natural", elongated conformation of an intact mucin.

MATERIALS AND METHODS

Mucin Purification and Reconstitution. Porcine gastric mucin was purified as previously described.[31] In brief, pig stomachs were gently rinsed with tap water, and mucus was harvested by manually scraping the gastric mucosa with spoons. The collected mucus was diluted 5-fold in 10 mM sodium phosphate buffer (pH 7.0) containing 170 mM NaCl and 0.04% (w/v) NaN_3. After homogenization at 4 °C overnight, cellular debris was removed *via* two centrifugation steps (first at 8300*g* and 4 °C for 30 min, second at 15,000*g* and 4 °C for 45 min) and a final ultracentrifugation step (150,000*g* and 4 °C for 1 h). Subsequently, the mucins were isolated by means of size exclusion chromatography using an ÄKTA purifier system (GE Healthcare, Chicago, IL, USA) and an XK50/100 column packed with Sepharose 6FF. The obtained mucin fractions were pooled, dialyzed against ultrapure water, and concentrated by cross-flow filtration using a membrane with a molecular weight cut-off of 100 kDa (GE Healthcare). The concentrate was then lyophilized and stored at −80 °C until further usage. To reconstitute mucin solutions, the lyophilized mucin powder was dissolved in ultrapure water while shaking at 4 °C for 1 h. Since we do not add any reducing agent to the harvested mucus, we expect our lab-purified mucin to contain both monomeric mucin molecules and mucin oligomers. We have demonstrated previously that—in either state—our lab-purified mucin is of superior quality compared to commercial porcine gastric mucin.[15] Moreover, a mass spectrometer analysis of our lab-purified mucin solution has shown that, whereas molecular contaminants are still present, MUC5AC is (in terms of identified matches with the generated fragments) the most frequent protein in the purified product.

Enzymatic Treatment of Mucins. Mucin that is purified from gastric mucus is always associated with DNA, and this might be the physiological state gastric mucins occur in. This DNA, however, can be removed efficiently by an enzymatic treatment as indicated by a gel electrophoresis with subsequent DNA staining (Figure S1a). For enzymatic removal of mucin-associated DNA, lyophilized MUC5AC powder was first exposed to UV radiation for 1 h and then dissolved in sterile 50 mM Tris−HCl (AppliChem, Darmstadt, Germany and Carl Roth, Karlsruhe, Germany) buffer (pH 7.5) supplemented with 10 mM $MgCl_2$ (Carl Roth) at a concentration of 1 mg mL^{-1}. Per 1 mg mucin, 50 μL of a 0.1% (w/v) bovine pancreas deoxyribonuclease I (DNase I) solution (Sigma-Aldrich, St. Louis, USA) was mixed with the mucin solution and incubated at 37 °C overnight while shaking at 250 rpm (Promax 1020, Heidolph Instruments GmbH & Co. KG, Schwabach; Germany). This DNase-treated mucin was then further purified as described above.

Afterward, some of the DNase-treated mucin was further treated with sulfatase (which we checked for proteinase-activity as shown in Figure S1b): again, the DNA-reduced mucin was exposed to UV light for 1 h and then dissolved in sterile 200 mM sodium acetate buffer (pH 5.0). Per 1 mg of mucin, 1 U sulfatase from *Helix pomatia* (type H-1, Sigma-Aldrich, St. Louis, MO, USA) was added. The reaction was allowed to take place at 37 °C overnight while shaking at 250 rpm (Heidolph Instruments GmbH & Co. KG). Also here, the modified mucin was further purified as described above. Using a commercial kit for quantification of the released sulfate groups (QuantiChrom Sulfate Assay; BioAssay Systems, Hayward, CA, USA), we have determined previously that the removed sulfate motifs account to ∼1.35% of the mucin dry weight.[15] For another batch of lab-purified gastric mucin, we found that, with the same enzymatic treatment, ∼0.9 ± 0.1% of the mucin dry weight was removed; this agrees well with both literature values[32,33] and our previous experimental results.[15] We note that the sulfatase used in this study is an arylsulfatase. Mucins, however, do not carry aryl sulfate groups but a significant amount of *N*-acetylglucosamine-6-sulfate (GlcNAc-6-SO_3) groups.[34,35] We verified the activity of the arylsulfatase against this specific motif by repeating the sulfate assay using heparin as a substrate, which also carries such GlcNAc-6-SO_3 groups. The sulfate groups removed by this treatment account to ∼0.56 ± 0.02% of the heparin dry weight. Given that each disaccharide unit of heparin, on average, carries 2−2.5 sulfate groups,[36] this suggests that the activity of the enzyme used here against GlcNAc-6-SO_3 groups is rather low.

Depletion Assay. To determine relative binding affinities of molecules toward different mucin variants, a depletion assay was conducted as recently described (Figure 1a).[37] As unspecific binding

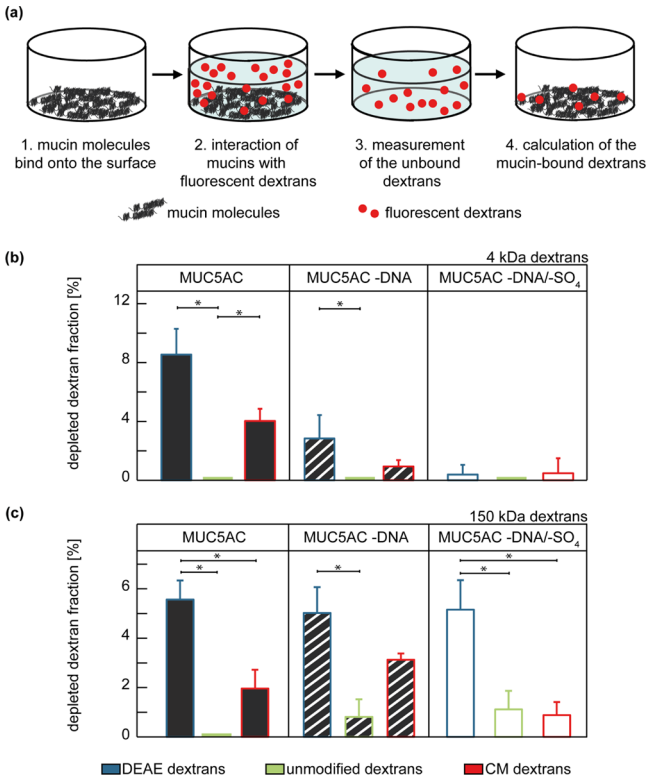

Figure 1. Depletion assay to assess the binding interaction of native and enzymatically treated mucins with different dextrans. (a) Schematic representation of the experimental setup used for the depletion assay. Mucins are passively adsorbed onto the bottom and lateral wall of wells of a well plate. Then, a solution of fluorescently labeled dextrans is added, from which dextrans are depleted by binding to the adsorbed mucin layer. Finally, the fluorescence intensity of the supernatant (which contains the remaining, i.e., unbound dextrans) is determined, from which the amount of depleted (=mucin bound) dextrans can be derived. (b,c) Binding of cationic (blue), neutral (green), and anionic (red) dextrans to adsorbed mucin layers is compared for dextrans with a molecular weight of 4 (b) and 150 kDa (c). The error bars represent the standard error of the mean as obtained from five individual samples. Asterisks mark significant differences between the dextran groups ($p \leq 0.05$) determined by one-way ANOVA combined with a Tukey post-hoc test for pairwise comparison.

partners for mucins, we selected dextrans since these polysaccharides are easy to handle and available as different variants, for example, with different functionalizations but similar molecular weights. In addition to six different dextran species (MW: 4 and 150 kDa, respectively; three variants per MW: diethylaminoethyl-modified, unmodified, and carboxymethyl-(CM-) modified; each conjugated with fluorescein isothiocyanate (FITC); Sigma-Aldrich), also the FITC-conjugated

https://dx.doi.org/10.1021/acs.langmuir.0c02256
Langmuir 2020, 36, 12973−12982

lectin wheat germ agglutinin (WGA, which binds to sialic acid motifs) was tested. Dextrans with a molecular weight of 4 kDa were dissolved in 20 mM HEPES buffer (pH 7.0) at a concentration of 0.02% (w/v), dextrans with a molecular weight of 150 kDa at a concentration of 0.00125% (w/v) in the same buffer. The WGA was dissolved at a concentration of 10 μg mL^{-1} in 20 mM HEPES buffer (pH 7.0).

Then, wells of a 96-well microtiter plate (Corning, Inc., Corning, NY, USA) were coated with mucin molecules by means of passive adsorption. For this purpose, 0.1% (w/v) mucin was dissolved in 20 mM HEPES buffer (pH 7.0), and 200 μL of this mucin solution was added to each well; then, incubation was conducted at 4 °C overnight. Afterward, the wells were rinsed with 200 μL of 20 mM HEPES buffer twice, and each well was incubated with 200 μL of a test molecule solution at RT for 1 h. After incubation, 100 μL of the test molecule solution was transferred from each well into a fresh well of an uncoated 96-well microtiter plate, and the fluorescence intensity of each sample was measured with a multi-label plate reader (Viktor3, PerkinElmer, Inc., MA, USA) at a wavelength of 535 nm using a data acquisition time of 0.1 s. Normalization of these measured fluorescence values was then conducted as follows: for each ligand molecule tested here (*i.e.*, either a dextran variant or WGA), both mucin-coated and uncoated wells were filled with equal amounts of the respective ligand solution and incubated as described above. Then, average values were determined for the fluorescence signal measured for samples from coated and uncoated wells, and the ratio of those values was calculated.

Fluorescence Labeling of Mucins. The three mucin variants were each labeled with the green fluorescent dye ATTO488 (carboxy-modified, ATTO-TEC GmbH, Siegen, Germany). 5 mM 1-ethyl-3(3-dimethyl-aminopropyl)-carbodiimide and 10 mM sulfo-*N*-hydroxysuccinimide (sulfo-NHS) were mixed with the fluorescent dye at a concentration of 1 mg mL^{-1} in 10 mM 2-(*N*-morpholino)-ethanesulfonic acid buffer (pH 5.0). After an incubation time of 3 h at room temperature, 100 μL of this mixture was added to a 0.2% (w/v) solution of mucins (dissolved in Dulbecco's phosphate-buffered saline solution = DPBS; Lonza, Verviers, Belgium). The activated, carboxy-modified fluorophore is covalently coupled to the amine groups of the mucin molecule by incubation at room temperature for 3 h. The ATTO488-labeled mucins were then further purified as described above for native mucin. Solutions of the fluorescently labeled mucin variants were prepared in 20 mM HEPES buffer (pH 7.0) and incubated in the wells of a 96-well plate in a concentration series ranging from 0.001 to 0.1% (w/v) at 4 °C overnight. The fluorescence intensity of each mucin solution was determined with a multi-label plate reader (Viktor3) at a wavelength of 535 nm using a data acquisition time of 0.1 s.

Indirect Enzyme-Linked Immunosorbent Assay. For ELISA experiments, first, five wells of a 96-well microtiter plate (Corning, Inc., Corning, NY, USA) were incubated with a solution containing a particular mucin variant [0.01% (w/v) mucin in PBS] each. After an incubation step conducted at room temperature for 2 h, the wells were washed three times with PBS and then blocked with PBS-Tween [0.1% Tween 20, Carl Roth, pH 7.4, supplemented with 5% (w/v) milk powder] at 4 °C overnight. After washing the wells with PBS-Tween, the primary antibody (ABIN966608, antibodies-online GmbH, Aachen, Germany, diluted 1:400 in blocking buffer) was added to each well. After incubating the samples at room temperature for 1 h while shaking at 100 rpm (Heidolph), the wells were washed with PBS-Tween again. Then, the secondary antibody [horse radish peroxidase (HRP) conjugated goat anti-mouse IgG antibody, ABIN237501, antibodies-online GmbH; diluted 1:5000 in blocking buffer] was added to the wells. The samples were incubated at room temperature for 2 h while shaking at 100 rpm and washed with PBS. Since the secondary antibody is conjugated to a HRP enzyme, 100 μL of the corresponding substrate (QuantaRed Working solution; QuantaRed Enhanced Chemifluorescent HRP Substrate Kit, Thermo Fisher Scientific, Waltham, MA, USA) comprising 50 parts QuantaRed Enhancer Solution, 50 parts QuantaRed Stable Peroxide, and one part QuantaRed ADHP Concentrate, was added to each well. Then, the samples were incubated at room temperature for 30 min while shaking at 100 rpm, and the peroxidase reaction was stopped by adding 20 μL QuantaRed Stop Solution to each well. Finally, the absorbance properties of the samples were determined photometrically with a multi-label plate reader (Viktor3) at an excitation wavelength of 570 nm.

Statistics. Statistical analyses were conducted using software R together with the user interface RStudio (version 3.4.2, September 2017). Normal distribution of data was verified by $Q-Q$ plots and a Shapiro–Wilk test, and variance homogeneity was confirmed using a Levene test. To detect statistically significant differences in the examined groups, *t*-tests were performed in pairwise comparisons. As a threshold for significance, a *p*-value of $p \leq 0.05$ was used.

Numerical Model and Methods. The numerical investigations conducted here aimed at investigating qualitative differences in the conformation of a mucin filament due to different effective line charge distributions. The simulations thus considered a single, initially straight mucin filament, which is modeled by a 3D beam theory and discretized in space by means of finite elements. Specifically, the geometrically exact Hermitian Simo–Reissner element formulation was applied here.[38] Thermal excitation and viscous damping of the filament due to the implicitly modeled surrounding fluid were incorporated *via* the micromechanical continuum approach to Brownian dynamics.[39] The electrostatic (self-)interaction of the mucin filament was modeled by the so-called section–section interaction potential (SSIP) approach.[40] Steric repulsive forces due to (self-)contact of the filament were accounted for by means of the penalty beam contact formulation[41] and precluded any mutual penetration. The challenging combination of this beam contact formulation with the possibly attractive electrostatic forces from the SSIP approach has been verified in previous work.[40,42] The software package used for the simulations is the in-house research code BACI.[43] Further details on the models and the simulation setup including all parameter values can be found in Section S3.3 of Supporting Information.

RESULTS AND DISCUSSION

Binding Capability of Small Charged Molecules toward Mucins is Modulated by the Mucin Charge Density. Previously, we could show that binding interactions between native mucins and charged dextran molecules are dominated by attractive electrostatic forces: charged dextrans with a molecular weight of 4 kDa bind to mucins, whereas uncharged dextrans do not.[37] Here, we repeat this adsorption-based affinity assay using the same three 4 kDa dextran variants and confirm the result from our previous study (Figures 1 and S2). Both cationic and anionic dextrans bind to surface-bound mucin layers in a concentration-dependent manner; in contrast, we do not find such a concentration dependency for neutral dextrans, which show low binding at all the concentrations tested (Figure S3). In addition, cationic dextrans tend to show a slightly higher (but not statistically significant; $p = 0.09$ for Figure 1 and $p = 0.07$ for Figure S2) MUC5AC binding capability than anionic ones. Determining K_D values for the binding of the different dextran variants to our lab-purified mucins is, however, challenging for conceptual and technical reasons: First, the binding of dextrans to binding sites of the mucin molecule can be strongly influenced by previous binding events. For instance, binding of dextrans to the mucin molecule can alter the (local) charge state of the mucin molecule; this, in turn, can result in conformational changes of certain domains of the mucin molecule. Second, we find that binding data obtained at high ligand concentrations comes with larger experimental errors, which renders a fitting procedure of those curves unreliably. This increased experimental variability may—at least in part—reflect the complex consequences multiple binding events can have on the

https://dx.doi.org/10.1021/acs.langmuir.0c02256
Langmuir 2020, 36, 12973–12982

mucin molecule. Thus, to avoid such complications, we here compare the binding of dextrans to different mucin variants at a low dextran concentration of 0.02% (w/v), where our molecular depletion test returns data with high accuracy.

In the next step, we ask if an enzymatic removal of anionic motifs from the mucin glycoprotein were to affect their adsorption efficiency onto hydrophobic surfaces and their dextran binding abilities. Thus, to clarify the first issue, we try to estimate the amount of surface-adsorbed mucin molecules based on an optical method. In brief, all three mucin variants are covalently labeled with a fluorophore targeting free amine residues on the mucin polypeptide backbone; then, these fluorescently labeled mucins are allowed to passively adsorb onto polystyrene surfaces, and the fluorescence intensity values of the adsorbed mucin surface layers are determined. Interestingly, we obtain differences in the labeling efficiencies of those three mucin variants which are already visible by eye (Figure S4a). The fluorescence signals of mucin solutions of the enzymatically modified mucins are similar, whereas the native mucin differs significantly with ∼4 fold higher fluorescence intensities (Figure S4b). Afterward, we investigate the relative adsorption efficiency of the three mucin variants by quantifying fluorescence microscope images (see Figure S4c). After correcting for differences in the fluorophore labeling efficiency, we find that the MUC5AC -DNA/-SO_4 variant shows the strongest surface adsorption among all mucin variants. In addition, QCM-D measurements (Figure S4d) show that the presence of a fluorescent dye on the mucin does not significantly influence the adsorption of mucin molecules onto hydrophobic surfaces.

With this mucin adsorption data in mind, the interaction of surface-bound mucins with solubilized dextrans could be affected by three aspects: differences in the amount of surface-bound mucin molecules, structural motifs on the mucin glycoprotein, and mucin-bound DNA. For instance, mucin-bound DNA may interact with the predominantly positively charged termini of the mucin protein backbone and thus influence its interaction with dextran molecules. We here compare the influence of two enzymatic mucin modifications: First, we test mucins from which associated DNA was removed; second, we analyze mucins, where—in addition to DNA removal—also sulfate residues were cleaved.

When we compare the binding behavior of the three dextran variants to DNA-free mucins, a qualitatively similar result is obtained as for untreated mucins; however, now, we only find slightly better binding of charged dextrans than for uncharged dextrans (Figure 1). This is interesting since the removal of anionic DNA strands from the mucin glycoprotein should have decreased intermolecular repulsion forces acting between the mucin backbone and the anionic dextrans, which—in turn—should have facilitated binding of anionic dextrans rather than weakening it. If sulfate groups are removed from mucins as well, the picture is further modified: now, both charged dextrans show negligible binding at levels as low as for uncharged dextrans (Figure 1). For cationic dextrans, this result can be rationalized as anionic motifs such as sulfate residues constitute a very likely target for the unspecific binding of cationic molecules. For the anionic dextrans, however, this outcome—albeit reproducible (Figure S2)—requires further investigation.

Thus, the same assay is repeated with a similar set of dextrans carrying the same chemical modifications (thus, representing the same set of charge species) but having larger molecular weights of 150 kDa. With these larger dextrans, the results obtained after enzymatic treatment are very similar to what we described above for binding of small 4 kDa dextrans: also here, CM-dextrans do not show significant binding to mucins anymore once the mucin-associated DNA and sulfate groups are removed. However, we would like to mention that this experimental outcome of molecular binding tests can depend on the mucin purification batch.[37] For a complex biological macromolecule as mucin, this is not surprising as the glycosylation pattern of mucin glycoproteins is subject to a certain degree of biological variability: the glycosylation of MUC5AC molecules can vary not only between individual pigs[44] (from whose stomachs we purify our mucins) but also within one and the same animal depending on its health state and diet.[45] As a consequence, we also find slight variations in the dextran binding patterns when different purification batches of our lab-purified mucin are compared (Figure S2).

Considering the counterintuitive outcome of the mucin binding tests conducted with CM-dextrans in the depletion assay, we next try to verify this result with other quantitative experimental techniques. We choose two adsorption-based assays to test dextran binding to the different mucin variants, that is, QCM-D measurements (Figure S5) and polydimethylsiloxane (PDMS)-based capillary filter systems (Figure S6).[46] In both cases, the surfaces are functionalized with mucin molecules and, in the second step, the dextrans are selectively depleted from the solution by the surface-bound mucins. Also with those two techniques, we find that the binding of positively charged dextrans to native mucin molecules is very pronounced, whereas the anionic and neutral dextrans are depleted to a much lower extent (Figures S5 and S6). Moreover, also as shown in Figure S5, those additional experiments confirm that glycan-reduced mucins do not bind anionic dextrans anymore.

Taken together, all these experiments indicate that—in addition to removing binding sites for cationic molecules—an enzymatic cleavage of anionic residues from mucin glycoproteins also affects the binding capability of mucins toward anionic molecules. At this point, it is important to recall that the most likely target motifs on mucins, which could allow for the binding of those anionic molecules, are located in the termini of the mucin glycoprotein, that is, in the unglycosylated areas of the peptide backbone. If the conformation of the (largely unfolded) mucin is well elongated, that is, if those termini are accessible, then binding to those terminal groups should be easily possible. In turn, conformational changes as, for example, brought about by weakened intramolecular repulsion forces (as we expect them for sulfate-reduced mucins), could reduce the accessibility of these termini—thus lowering the efficiency of anionic CM-dextran binding. In fact, previous experiments on the adsorption properties of native and enzymatically modified mucins had already motivated that the mucin macromolecule might undergo such a conformational change upon removal of negatively charged residues from the backbone.[15]

Anionic Groups on the Mucin Backbone Modulate the Conformation of the Mucin Glycoprotein. To test the idea that mucin macromolecules adopt a different, more contracted conformation upon removal of anionic charges from the backbone, we employ numerical simulations of the mucin molecule. Our goal is to compare structural parameters of thermally fluctuating mucins that describe the configuration

https://dx.doi.org/10.1021/acs.langmuir.0c02256
Langmuir 2020, 36, 12973−12982

of the macromolecule—both in the presence and absence of negative charges within the mucin backbone.

To set up a numerical model of the complex mucin glycoprotein, we first segment the macromolecule into different subunits. This approach is motivated by the presence of different structural motifs in the porcine gastric mucin (Figure 2a): MUC5AC comprises a strongly glycosylated core-

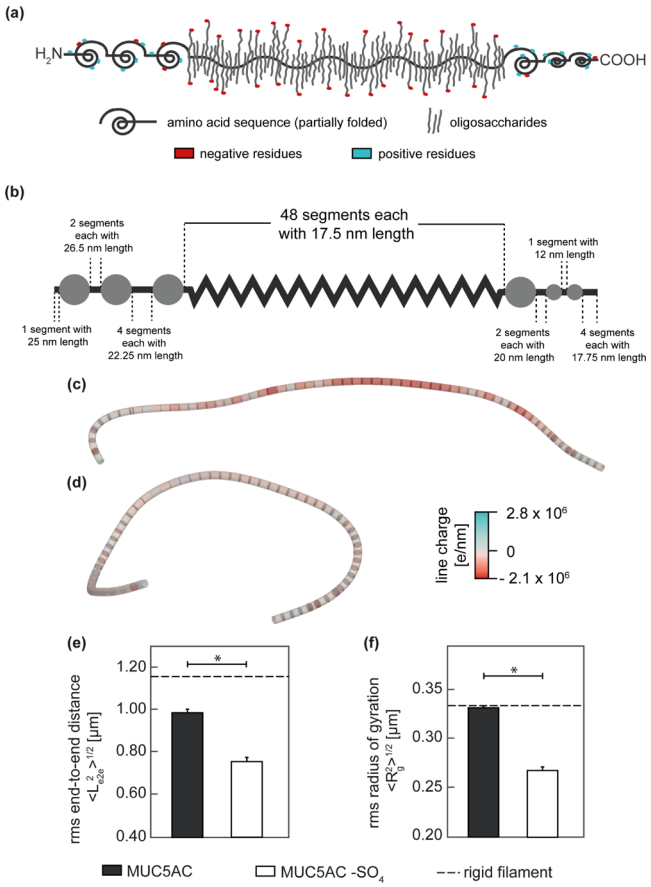

Figure 2. Schematic representation of a mucin macromolecule and numerical simulation results obtained for native and enzymatically treated mucin. (a) Schematic structure of the mucin glycoprotein and its charge distribution. (b) The segmentation of the mucin molecule conducted for modeling results in 48 units for the glycosylated region, whereas each terminus is represented by three units modeling the VWF-like, folded domains and seven connecting segments. Representative examples of the modeled conformation of native and sulfate-reduced (MUC5AC -SO_4) mucin are shown in (c,d), respectively. The corresponding structural parameters, that is, the end-to-end distance and the radius of gyration as calculated from the simulated mucins are shown in (e,f). The error bars depict the standard error of the mean as obtained from five independent simulation runs. Asterisks mark significant differences ($p \leq 0.05$).

domain which is flanked by partially folded termini. These termini contain three von-Willebrand-factor (VWF)-like D domains in the *N*-terminus and one VWF-like D domain as well as two VWF-like C domains in the C-terminus. We here simplify this structure and model these spherical VWF-like domains as cylinders (Figure 2b), which are connected by other cylindrical segments corresponding to the respective protein strands (see Supporting Information, Section S3.1 for details). The central, glycosylated region of the mucin is broken down into 48 segments of 50 amino acids each, and each of these segments was treated as a beam element with a persistence length of 50 nm.[27,47] Then, a longitudinal charge profile was applied onto the segmented mucin glycoprotein as described in Section S3.2 of Supporting Information. Of course, this is still a simplified model of the mucin glycoprotein, which is why the absolute numbers of the quantities we determine from the simulated mucin molecules below should be considered to be estimates.

Interestingly, for simulated mucin at neutral pH, we obtain average end-to-end distances and radii of gyration that are close to values one would obtain for a rigid, well-elongated molecule. This finding indicates that the high density of negatively charged groups in the central area of the mucin macromolecule establishes rather strong (intramolecular) repulsive forces, which keep the polypeptide in a stretched conformation (Figure 2c). We then challenge the validity of the numerical mucin model by comparing the conformation of an enzymatically untreated mucin (neglecting any mucin-associated DNA) at neutral and acidic pH. This step is motivated by experimental results from the literature, which have reported a clear compaction of the mucin glycoprotein when the pH level of the solvent was decreased from 7.0 to 2.0.[28,48] Indeed, this behaviour is reproduced here (Figure S7): when mucin charge profiles corresponding to neutral and acidic buffer conditions are applied in our model, we find a reduction of both the end-to-end distance and the radius of gyration of simulated mucins by a factor of ∼4.5 and ∼2, respectively.

Having confirmed that our model can successfully reproduce charge-driven conformational changes (induced by alterations in the pH) reported in the literature, we next ask if the same model would predict a conformational change of the mucin macromolecule when anionic residues are removed. In these simulations, we can test the influence of two modifications, that is, removal of either sulfate residues (Figure 2) or sialic acid groups (Figure S8). However, mucin-associated DNA cannot be simulated since it is unclear which part of the mucin molecule DNA binds to. Thus, the MUC5AC -DNA molecule serves as a reference here. The conformational change depicted in the simulated mucins might thus underestimate the structural alteration native mucins undergo upon removal of both DNA and anionic glycans.

Indeed, when anionic sulfate groups are removed from the charge profile used for modeling, we obtain a compacted mucin conformation (Figure 2d) as demonstrated by both a significant reduction of the end-to-end distance (Figure 2e) and the radius of gyration (Figure 2f). We conclude that a loss of repulsive forces between the glycan chains forces the mucin to adopt a compacted conformation. For simulated mucins, where the anionic motifs originating from sialic acid groups were removed, we find the same outcome—albeit more weakly pronounced (Figure S8c,d). This reflects the lower density of sialic acid groups on the mucin glycoproteins compared to sulfate residues.[15]

At this point, we would like to emphasize again that the numerical model we chose to describe the mucin conformation reflects a simplified scenario. It allows for making statements on the conformational changes of monomeric mucins only; yet, physiologically, gastric mucins typically occur in an oligomeric state. Such a simplification, however, is still reasonable, given that our lab-purified mucins return a similar interaction pattern with dextrans in their reduced, monomeric state as in their oligomerized state (Figure S9). Indeed, the

https://dx.doi.org/10.1021/acs.langmuir.0c02256
Langmuir 2020, 36, 12973−12982

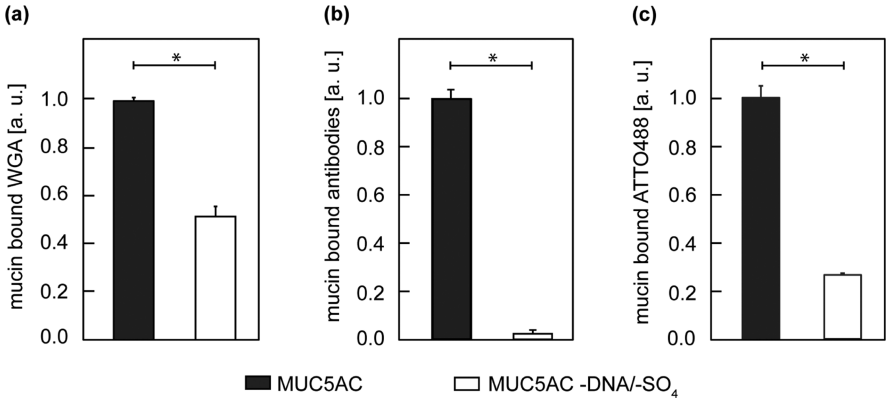

Figure 3. ELISA test, depletion assay, and ATTO488 labeling efficiency to assess the interaction of native and enzymatically treated mucins with specific binding partners. WGA (a), anti-MUC5AC antibodies, (b) and fluorescent dye molecules (c) show a higher binding capability toward native mucin (MUC5AC) than toward the enzymatically modified mucin variants. The error bars represent the standard error of mean obtained from five (ELISA and depletion assay) and three (ATTO488 labeling) technical replicates. Asterisks mark significant differences between samples ($p \leq 0.05$).

conformational changes we propose here for monomeric mucins upon removal of charges from the mucin backbone might be even more pronounced in mucin oligomers: here, conformational changes occurring for individual mucin molecules might add-up, thus resulting in a more strongly decreased accessibility of the mucin termini than what we estimate with our mucin model.

Removal of Anionic Mucin Motifs Affects the Accessibility of Specific Mucin-Binding Sites. Having demonstrated that the removal of sulfate groups should indeed be sufficient to induce a significant change in the mucin confirmation, we now, in the last step, ask if specific binding interactions with mucins are also affected by the enzymatic cleavage of those anionic mucin residues and the ensuing mucin compaction. At this point, it is crucial to recall that our enzymatic treatment targets DNA strands and sulfate groups only. Thus, cleaving those chemical motifs is unlikely to chemically remove target groups on mucins required for binding of the WGA, a molecule that binds specifically to sialic acid groups.

Interestingly, when we repeat the depletion assay described above using this specific lectin variant as a binding partner for mucin, we find that the amount of WGA that is depleted by MUC5AC from a WGA solution exceeds the amount of WGA that is depleted by MUC5AC -DNA/-SO_4 by a factor of ∼2 (or ∼5, respectively), and this difference is statistically significant (Figure 3a; Figure S10). Thus, this finding indicates lower WGA binding to the sulfate-reduced mucin.

We obtain a qualitatively similar result as for the WGA binding test described above when we perform an ELISA test, that is, another specific mucin binding assay which is based on an anti-MUC5AC antibody, which targets the C-terminus of the mucin molecule.[49] Whereas the antibody returns a strong fluorescence signal for native mucin, a ∼20-fold weaker signal is detected for the enzymatically modified mucin (Figures 3b and S10).

At this point, it is important to recall that these adsorption-based binding tests—as well as the depletion assay that we have discussed above—come with the complication that native MUC5AC and MUC5AC -DNA/-SO_4 differ in terms of adsorption efficiency. As mentioned above, first, we analyzed the labeling efficiency of native MUC5AC and enzymatically treated MUC5AC -DNA/-SO_4. The fluorescence intensities of aqueous solutions generated with these two labeled mucins differ significantly: we obtain a ∼4 fold weaker fluorescence signal for the enzymatically treated mucin variant (Figures 3c and S4b). In full agreement with the results obtained with the anti-MUC5AC antibody and WGA, this underscores that specific binding sites on glycan-depleted mucins are less accessible. Moreover, the relative ratio of surface-bound native and enzymatically modified mucins is determined by fluorescence microscopy. The data shows stronger adsorption for MUC5AC -DNA/-SO_4 than for the untreated mucin (Figure S4c). With this in mind, the relative binding differences shown in Figure 3 represent an underestimation; in other words, the reduction in accessibility of specific binding sites can be expected to be stronger than what the data shown in Figure 3 suggests.

Together, this data suggests that also binding of specific binding partners to mucin is rendered more difficult when a sufficient number of anionic groups are removed from the glycoprotein. Also, this finding is consistent with the idea that a loss of intramolecular repulsion forces in the glycosylated domain induces conformational changes of the mucin structure such that certain mucin motifs (including the cationic C-terminus of the macromolecule) are hidden in the coiled-up mucin and thus become less accessible for binding partners.

In summary, both our numerical model and the experimental data imply that the native MUC5AC exhibits a stretched and elongated conformation, whereas the enzymatic modifications studied here yield mucins with a more compacted, globular structure, in which the mucin termini are (partially) shielded from the surrounding fluid. Of course, our numerical model comes with limitations: for instance, DNA-associated mucin cannot be simulated, and thickness variations along the backbone of the mucin glycoprotein (*i.e.*, between glycosylated and unglycosylated regions) are not considered. Thus, the visualization of the mucin molecules in Figure 2c,d does not necessarily indicate the full effect of how binding sites on the modified mucin become inaccessible for other small molecules.

Yet, the idea put forward here is in agreement with our previous result where we found that an enzymatic removal of mucin-associated DNA and sulfate groups from the mucin glycan chains impairs the functionality of mucins in terms of lubricity and adsorption efficiency.[15] Here, we show that the

https://dx.doi.org/10.1021/acs.langmuir.0c02256
Langmuir 2020, 36, 12973−12982

same mucin modifications lead to an altered binding capability of mucins toward charged molecules—both cationic and anionic ones—and proteins, which specifically bind to certain motifs of the mucin molecule (Figure 4).

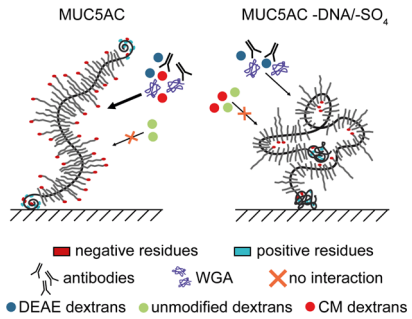

Figure 4. Schematic representation of how removal of anionic residues could affect the conformation of MUC5AC and thus the accessibility of mucin binding sites. Native gastric mucin can bind the anti-MUC5AC antibody, WGA, and charged dextrans but not electrostatically neutral dextrans. In contrast, enzymatically treated (charge-reduced) MUC5AC shows less efficient binding to antibodies and WGA and does not bind anionic dextrans anymore.

In this study, we use surface-bound mucins for all experimental and numerical tests. Indeed, in their physiological state, mucins can occur in the surface bound form; yet, they are also secreted and form solutions or gels. For interpreting the binding results presented here, using surface-bound mucins helps us avoiding certain technical complications: for instance, as dextran molecules carry multiple charges (~5 charges for the 4 kDa dextrans and ~185 charges for the 150 kDa dextrans), the polyanionic/polycationic character of those macromolecules could lead to intermolecular interactions of mucin molecules with each other (*e.g.*, triggered via cross-linking by the dextrans) and thus to the formation of agglomerates.[50]

Possible Physiological Role of MUC5AC-Associated DNA. We here study porcine gastric MUC5AC, which we purify manually in the lab. Interestingly, this lab-purified MUC5AC is always associated with DNA, and we could show previously that this mucin-associated DNA reduces the accessibility of sialic acids and sulfate groups on the mucin backbone towards enzyme.[15] Thus, before treating mucin with sulfatase, we first perform an enzymatic removal of DNA. In contrast to MUC5AC, lab-purified salivary mucin MUC5B hardly contains any DNA.[15] The content of sialic acid and sulfate groups in MUC5B, however, strongly exceeds that of MUC5AC: sialic acid and sulfate groups each account for ~6% of the mass of MUC5B but only for <2% of the mass of MUC5AC.[15,32,51,52] If we assume that the decoration of MUC5AC with DNA might not just be the result of the (relatively harsh) harvesting method used for collecting gastric mucus (which is collected by manual scraping of the gastric mucosa) but rather represents the physiological state of MUC5AC, the question arises if mucin-associated DNA might provide MUC5AC with additional or improved properties.

Based on the results we obtained in this study, we speculate that MUC5AC-associated DNA might compensate for the relatively low amount of sialic acid and sulfate residues present in this mucin variant compared to MUC5B. Thus, by its association with gastric mucin, DNA might help keeping the mucin glycoprotein in an extended state so that all of its (specific and unspecific) interaction sites are accessible. Whereas at neutral pH levels, as we study them here, the mucin can maintain an extended configuration on its own, at acidic pH levels, this is more difficult, which represent the physiological environment the gastric MUC5AC occurs in. With our model, we can predict that, at an acidic pH of 4.0, protonation of anionic residues on the polypeptide chain induces a compaction of the mucin molecule (Figure S7). Here, the phosphate groups from mucin-associated DNA strands, however, might still be deprotonated (given that the pK_a value of phosphate groups in phosphodiester bonds is close to 1),[53] thus adding negatively charged groups and, consequently, intramolecular repulsion forces to the mucin glycoprotein. However, as neither the detailed amount of DNA bound per mucin nor the position on the mucin glycoprotein where DNA strands bind to are known, it is—at this point of research—very difficult to include this aspect into our numerical mucin model.

It is reasonable to assume that DNA strands are likely to bind via electrostatic forces to positively charged amino acid side chains that are located in the mucin termini. The high density of anionic glycan chains might render binding of polyanionic DNA molecules to the central region difficult. Other DNA binding mechanisms, for example, *via* physical entanglement with glycan side chains or *via* hydrogen bonds, are, of course, also possible.[54] When attached to mucin, DNA strands might not only help stretching the mucin molecule but also act as a protective barrier against enzymatic attack from pathogens: indeed, several bacteria or viruses have developed strategies to enzymatically target mucin motifs.[55,56] For instance, sialic acid residues are known as binding sites for influenza viruses[57,58] and are thus targeted by viral neuraminidases to set immobilized viruses free again.[59] Moreover, some bacteria residing in airway or gastrointestinal mucus secrete sulfatases,[21,32,60]—and, as we show here, the removal of sulfate residues alters the mucin conformation and affects mucin functionality. How the protective barrier function of mucus-containing such charge-reduced, collapsed mucins might be corrupted due to the inaccessibility of certain mucin-binding sites will have to be clarified in future experiments.

■ CONCLUSIONS

The biochemical structure of mucin glycoproteins is highly complex, and the particular role of the different glycans present in mucins remains to date poorly understood. Electrostatically neutral carbohydrates such as mannose, fucose, *N*-acetyl-galactosamine, *N*-acetyl-glucosamine, or galactose comprise the main components of the mucin glycan pattern and have been shown to constitute a protective barrier against proteolytic degradation of the polypeptide backbone.[61−63] Here, we suggest that anionic glycan residues contribute to the conformational stability of mucins by establishing intramolecular repulsion, and these repulsion forces seem to be required to maintain the broad binding properties of mucins toward other molecules. Future research will show if and how other mucin glycans contribute to similar or other properties of the complex mucin glycoprotein, including selective binding, surface adsorption, or bacterial/eukaryotic repulsion.

■ ASSOCIATED CONTENT

Supporting Information

The Supporting Information is available free of charge at https://pubs.acs.org/doi/10.1021/acs.langmuir.0c02256.

https://dx.doi.org/10.1021/acs.langmuir.0c02256
Langmuir 2020, 36, 12973−12982

SDS-PAGE to show the successful enzymatic modification of mucin molecules; experimental repetitions of the depletion assay with dextrans, WGA, and anti-MUC5AC antibodies; analysis of the mucin−dextran interaction with different assays: depletion assay with increasing dextran concentrations, QCM-D measurements, and selective PDMS filters; quantification of the relative amount of surface-bound mucin (ATTO-labeled mucins); details of the numerical model; and conformational change of the simulated natural mucin at different pH levels and of the enzymatically treated mucins at physiological pH (PDF)

AUTHOR INFORMATION

Corresponding Author

Oliver Lieleg − *Department of Mechanical Engineering and Munich School of Bioengineering, Technical University of Munich, 85748 Garching, Germany;* orcid.org/0000-0002-6874-7456; Email: oliver.lieleg@tum.de

Authors

Theresa M. Lutz − *Department of Mechanical Engineering and Munich School of Bioengineering, Technical University of Munich, 85748 Garching, Germany*

Matthias Marczynski − *Department of Mechanical Engineering and Munich School of Bioengineering, Technical University of Munich, 85748 Garching, Germany*

Maximilian J. Grill − *Department of Mechanical Engineering and Institute for Computational Mechanics, Technical University of Munich, 85748 Garching, Germany*

Wolfgang A. Wall − *Department of Mechanical Engineering and Institute for Computational Mechanics, Technical University of Munich, 85748 Garching, Germany*

Complete contact information is available at: https://pubs.acs.org/10.1021/acs.langmuir.0c02256

Author Contributions

The experiments were designed by T.M.L., M.M., and O.L. T.M.L. and M.M. performed the experiments and analyzed the data. M.J.G. and W.A.W. developed the numerical model, ran the simulations, and analyzed the data. The manuscript was written by contributions of all authors.

Notes

The authors declare no competing financial interest.

ACKNOWLEDGMENTS

The authors thank Tobias Fuhrmann for assistance with mucin purification. This project was supported by the Deutsche Forschungsgemeinschaft (DFG) through grant LI 1902/9-1 awarded to O.L.

REFERENCES

(1) Khanvilkar, K.; Donovan, M. D.; Flanagan, D. R. Drug transfer through mucus. *Adv. Drug Delivery Rev.* **2001**, *48*, 173−193.

(2) Lai, S. K.; Wang, Y.-Y.; Hanes, J. Mucus-penetrating nanoparticles for drug and gene delivery to mucosal tissues. *Adv. Drug Delivery Rev.* **2009**, *61*, 158−171.

(3) Yakubov, G. E.; McColl, J.; Bongaerts, J. H. H.; Ramsden, J. J. Viscous boundary lubrication of hydrophobic surfaces by mucin. *Langmuir* **2009**, *25*, 2313−2321.

(4) Hoffmann, W. Regeneration of the gastric mucosa and its glands from stem cells. *Curr. Med. Chem.* **2008**, *15*, 3133−3144.

(5) Yildiz, H. M.; Carlson, T. L.; Goldstein, A. M.; Carrier, R. L. Mucus barriers to microparticles and microbes are altered in Hirschsprung's disease. *Macromol. Biosci.* **2015**, *15*, 712−718.

(6) Peatfield, A. C.; Richardson, P. S. The action of dust in the airways on secretion into the trachea of the cat. *J. Physiol.* **1983**, *342*, 327−334.

(7) Lo-Guidice, J.-M.; Périni, J.-M.; Lafitte, J.-J.; Ducourouble, M.-P.; Roussel, P.; Lamblin, G. Characterization of a sulfotransferase from human airways responsible for the 3-O-sulfation of terminal galactose in N-acetyllactosamine-containing mucin carbohydrate chains. *J. Biol. Chem.* **1995**, *270*, 27544−27550.

(8) Parsons, C. L.; Mulholland, S. G. Bladder surface mucin. Its antibacterial effect against various bacterial species. *Am. J. Pathol.* **1978**, *93*, 423.

(9) Belley, A.; Göttke, M.; Keller, K.; Chadee, K.; Göettke, M. Intestinal mucins in colonization and host defense against pathogens. *Am. J. Trop. Med. Hyg.* **1999**, *60*, 10−15.

(10) Scharfman, A.; Lamblin, G.; Roussel, P. Interactions between human respiratory mucins and pathogens. *Biochem. Soc. Trans.* **1995**, *23*, 836−839.

(11) Yolken, R. H.; Peterson, J. A.; Vonderfecht, S. L.; Fouts, E. T.; Midthun, K.; Newburg, D. S. Human milk mucin inhibits rotavirus replication and prevents experimental gastroenteritis. *J. Clin. Invest.* **1992**, *90*, 1984−1991.

(12) Altgärde, N.; Eriksson, C.; Peerboom, N.; Phan-Xuan, T.; Moeller, S.; Schnabelrauch, M.; Svedhem, S.; Trybala, E.; Bergström, T.; Bally, M. Mucin-like region of herpes simplex virus type 1 attachment protein glycoprotein C (gC) modulates the virus-glycosaminoglycan interaction. *J. Biol. Chem.* **2015**, *290*, 21473−21485.

(13) Bansil, R.; Turner, B. S. Mucin structure, aggregation, physiological functions and biomedical applications. *Curr. Opin. Colloid Interface Sci.* **2006**, *11*, 164−170.

(14) Käsdorf, B. T.; Weber, F.; Petrou, G.; Srivastava, V.; Crouzier, T.; Lieleg, O. Mucin-inspired lubrication on hydrophobic surfaces. *Biomacromolecules* **2017**, *18*, 2454−2462.

(15) Marczynski, M.; Balzer, B. N.; Jiang, K.; Lutz, T. M.; Crouzier, T.; Lieleg, O. Charged glycan residues critically contribute to the adsorption and lubricity of mucins. *Colloids Surf., B* **2020**, *187*, 110614.

(16) Yakubov, G. E.; Papagiannopoulos, A.; Rat, E.; Easton, R. L.; Waigh, T. A. Molecular structure and rheological properties of short-side-chain heavily glycosylated porcine stomach mucin. *Biomacromolecules* **2007**, *8*, 3467−3477.

(17) McColl, J.; Yakubov, G. E.; Ramsden, J. J. Complex desorption of mucin from silica. *Langmuir* **2007**, *23*, 7096−7100.

(18) Copeman, M.; Matuz, J.; Leonard, A. J.; Pearson, J. P.; Dettmar, P. W.; Allen, A. The gastroduodenal mucus barrier and its role in protection against luminal pepsins: The effect of 16, 16 dimethyl prostaglandin E2, carbopol-polyacrylate, sucralfate and bismuth subsalicylate. *J. Gastroenterol. Hepatol.* **1994**, *9*, S55−S59.

(19) Chang, M.; Alsaigh, T.; Kistler, E. B.; Schmid-Schönbein, G. W. Breakdown of Mucin as Barrier to Digestive Enzymes in the Ischemic Rat Small Intestine. *PLoS One* **2012**, *7*, No. e40087.

(20) Hoskins, L. C.; Boulding, E. T. Mucin degradation in human colon ecosystems: evidence for the existence and role of bacterial subpopulations producing glycosidases as extracellular enzymes. *J. Clin. Invest.* **1981**, *67*, 163−172.

(21) Wright, D. P.; Rosendale, D. I.; Roberton, A. M. Prevotella enzymes involved in mucin oligosaccharide degradation and evidence for a small operon of genes expressed during growth on mucin. *FEMS Microbiol. Lett.* **2000**, *190*, 73−79.

(22) Roberton, A. M.; Corfield, A. P. Mucin Degradation and Its Significance in Inflammatory Conditions of the Gastrointestinal Tract. In *Medical Importance of the Normal Microflora*; Springer, 1999; pp 222−261.

(23) Crouzier, T.; Boettcher, K.; Geonnotti, A. R.; Kavanaugh, N. L.; Hirsch, J. B.; Ribbeck, K.; Lieleg, O. Modulating mucin hydration and

lubrication by deglycosylation and polyethylene glycol binding. *Adv. Mater. Interfaces* **2015**, *2*, 1500308.
(24) Zappone, B.; Patil, N. J.; Madsen, J. B.; Pakkanen, K. I.; Lee, S. Molecular structure and equilibrium forces of bovine submaxillary mucin adsorbed at a solid−liquid interface. *Langmuir* **2015**, *31*, 4524−4533.
(25) Rose, M. C.; Voter, W. A.; Sage, H.; Brown, C. F.; Kaufman, B. Effects of deglycosylation on the architecture of ovine submaxillary mucin glycoprotein. *J. Biol. Chem.* **1984**, *259*, 3167−3172.
(26) Kramer, J. R.; Onoa, B.; Bustamante, C.; Bertozzi, C. R. Chemically tunable mucin chimeras assembled on living cells. *Proc. Natl. Acad. Sci. U.S.A.* **2015**, *112*, 12574−12579.
(27) Shogren, R.; Gerken, T. A.; Jentoft, N. Role of glycosylation on the conformation and chain dimensions of O-linked glycoproteins: light-scattering studies of ovine submaxillary mucin. *Biochemistry* **1989**, *28*, 5525−5536.
(28) Hong, Z.; Chasan, B.; Bansil, R.; Turner, B. S.; Bhaskar, K. R.; Afdhal, N. H. Atomic force microscopy reveals aggregation of gastric mucin at low pH. *Biomacromolecules* **2005**, *6*, 3458−3466.
(29) Menchicchi, B.; Fuenzalida, J. P.; Hensel, A.; Swamy, M. J.; David, L.; Rochas, C.; Goycoolea, F. M. Biophysical analysis of the molecular interactions between polysaccharides and mucin. *Biomacromolecules* **2015**, *16*, 924−935.
(30) Co, J. Y.; Crouzier, T.; Ribbeck, K. Probing the Role of Mucin-Bound Glycans in Bacterial Repulsion by Mucin Coatings. *Adv. Mater. Interfaces* **2015**, *2*, 1500179.
(31) Schömig, V. J.; Käsdorf, B. T.; Scholz, C.; Bidmon, K.; Lieleg, O.; Berensmeier, S. An optimized purification process for porcine gastric mucin with preservation of its native functional properties. *RSC Adv.* **2016**, *6*, 44932−44943.
(32) Robinson, C. V.; Elkins, M. R.; Bialkowski, K. M.; Thornton, D. J.; Kertesz, M. A. Desulfurization of mucin by Pseudomonas aeruginosa: influence of sulfate in the lungs of cystic fibrosis patients. *J. Med. Microbiol.* **2012**, *61*, 1644−1653.
(33) Bhaskar, K. R.; Gong, D. H.; Bansil, R.; Pajevic, S.; Hamilton, J. A.; Turner, B. S.; LaMont, J. T. Profound increase in viscosity and aggregation of pig gastric mucin at low pH. *Am. J. Physiol.* **1991**, *261*, G827−G832.
(34) Xia, B.; Royall, J. A.; Damera, G.; Sachdev, G. P.; Cummings, R. D. Altered O-glycosylation and sulfation of airway mucins associated with cystic fibrosis. *Glycobiology* **2005**, *15*, 747−775.
(35) Amerongen, A. V. N.; Bolscher, J. G.; Bloemena, E.; Veerman, E. C. Sulfomucins in the human body. *Biol. Chem.* **1998**, *379*, 1−18.
(36) Shriver, Z.; Capila, I.; Venkataraman, G.; Sasisekharan, R. Heparin and Heparan Sulfate: Analyzing Structure and Microheterogeneity. In *Heparin-A Century of Progress*; Springer, 2012; pp 159−716.
(37) Marczynski, M.; Käsdorf, B. T.; Altaner, B.; Wenzler, A.; Gerland, U.; Lieleg, O. Transient binding promotes molecule penetration into mucin hydrogels by enhancing molecular partitioning. *Biomater. Sci.* **2018**, *6*, 3373−3387.
(38) Meier, C.; Grill, M. J.; Wall, W. A.; Popp, A. Geometrically exact beam elements and smooth contact schemes for the modeling of fiber-based materials and structures. *Int. J. Solids Struct.* **2018**, *154*, 124−146.
(39) Cyron, C. J.; Wall, W. A. Numerical method for the simulation of the Brownian dynamics of rod-like microstructures with three-dimensional nonlinear beam elements. *Int. J. Numer. Methods Eng.* **2012**, *90*, 955−987.
(40) Grill, M. J.; Wall, W. A.; Meier, C. A Computational Model for Molecular Interactions Between Curved Slender Fibers Undergoing Large 3D Deformations With a Focus on Electrostatic, van der Waals and Repulsive Steric Forces. *Int. J. Numer. Methods Eng.* **2020**, *121*, 2285−2330.
(41) Meier, C.; Popp, A.; Wall, W. A. A finite element approach for the line-to-line contact interaction of thin beams with arbitrary orientation. *Comput. Methods Appl. Mech. Eng.* **2016**, *308*, 377−413.
(42) Grill, M. J.; Meier, C.; Wall, W. A. Investigation of the peeling and pull-off behavior of adhesive elastic fibers via a novel computational beam interaction model. *J. Adhes.* **2019**, *95*, 1−30.
(43) Institute for Computational Mechanics *BACI: A Multiphysics Simulation Environment*; Institute for Computational Mechanics: Technical University of Munich, 2020.
(44) Karlsson, N. G.; Nordman, H.; Karlsson, H.; Carlstedt, I.; Hansson, G. C. Glycosylation differences between pig gastric mucin populations: a comparative study of the neutral oligosaccharides using mass spectrometry. *Biochem. J.* **1997**, *326*, 911−917.
(45) Padra, M.; Adamczyk, B.; Flahou, B.; Erhardsson, M.; Chahal, G.; Smet, A.; Jin, C.; Thorell, A.; Ducatelle, R.; Haesebrouck, F.; Karlsson, N. G.; Lindén, S. K. Helicobacter suis infection alters glycosylation and decreases the pathogen growth inhibiting effect and binding avidity of gastric mucins. *Mucosal Immunol.* **2019**, *12*, 784−794.
(46) Winkeljann, B.; Käsdorf, B. T.; Boekhoven, J.; Lieleg, O. Macromolecular Coating Enables Tunable Selectivity in a Porous PDMS Matrix. *Macromol. Biosci.* **2018**, *18*, 1700311.
(47) Round, A. N.; Berry, M.; McMaster, T. J.; Stoll, S.; Gowers, D.; Corfield, A. P.; Miles, M. J. Heterogeneity and Persistence Length in Human Ocular Mucins. *Biophys. J.* **2002**, *83*, 1661−1670.
(48) Maleki, A.; Lafitte, G.; Kjøniksen, A.-L.; Thuresson, K.; Nyström, B. Effect of pH on the association behavior in aqueous solutions of pig gastric mucin. *Carbohydr. Res.* **2008**, *343*, 328−340.
(49) Bara, J.; Chastre, E.; Mahiou, J.; Singh, R. L.; Forgue-Lafitte, M. E.; Hollande, E.; Godeau, F. Gastric M1 mucin, an early oncofetal marker of colon carcinogenesis, is encoded by the MUC5AC gene. *Int. J. Cancer* **1998**, *75*, 767−773.
(50) Marczynski, M.; Rickert, C. A.; Semerdzhiev, S. A.; Van Dijk, W. R.; Segers-Nolten, I. M. J.; Claessens, M. M. A. E.; Lieleg, O. α-Synuclein Penetrates Mucin Hydrogels Despite Its Mucoadhesive Properties. *Biomacromolecules* **2019**, *20*, 4332−4344.
(51) Loomis, R. E.; Prakobphol, A.; Levine, M. J.; Reddy, M. S.; Jones, P. C. Biochemical and biophysical comparison of two mucins from human submandibular-sublingual saliva. *Arch. Biochem. Biophys.* **1987**, *258*, 452−464.
(52) Henke, M. O.; John, G.; Germann, M.; Lindemann, H.; Rubin, B. K. MUC5AC and MUC5B mucins increase in cystic fibrosis airway secretions during pulmonary exacerbation. *Am. J. Respir. Crit. Care Med.* **2007**, *175*, 816−821.
(53) Thaplyal, P.; Bevilacqua, P. C. Experimental Approaches for Measuring pK_a's in RNA and DNA. *Methods in Enzymology*; Elsevier, 2014; Vol. *549*, pp 189−219.
(54) Wenz, C.; Jeltsch, A.; Pingoud, A. Probing the indirect readout of the restriction enzyme EcoRV mutational analysis of contacts to the DNA backbone. *J. Biol. Chem.* **1996**, *271*, 5565−5573.
(55) Corfield, A. P.; Wagner, S. A.; O'Donnell, L. J. D.; Durdey, P.; Mountford, R. A.; Clamp, J. R. The roles of enteric bacterial sialidase, sialateO-acetyl esterase and glycosulfatase in the degradation of human colonic mucin. *Glycoconjugate J.* **1993**, *10*, 72−81.
(56) Flynn, J. M.; Niccum, D.; Dunitz, J. M.; Hunter, R. C. Evidence and Role for Bacterial Mucin Degradation in Cystic Fibrosis Airway Disease. *PLoS Pathog.* **2016**, *12*, No. e1005846.
(57) Weis, W.; Brown, J. H.; Cusack, S.; Paulson, J. C.; Skehel, J. J.; Wiley, D. C. Structure of the influenza virus haemagglutinin complexed with its receptor, sialic acid. *Nature* **1988**, *333*, 426−431.
(58) Suzuki, Y.; Ito, T.; Suzuki, T.; Holland, R. E.; Chambers, T. M.; Kiso, M.; Ishida, H.; Kawaoka, Y. Sialic acid species as a determinant of the host range of influenza A viruses. *J. Virol.* **2000**, *74*, 11825−11831.
(59) Gubareva, L. V.; Kaiser, L.; Hayden, F. G. Influenza virus neuraminidase inhibitors. *Lancet* **2000**, *355*, 827−835.
(60) Rho, J.-h.; Wright, D. P.; Christie, D. L.; Clinch, K.; Furneaux, R. H.; Roberton, A. M. A novel mechanism for desulfation of mucin: identification and cloning of a mucin-desulfating glycosidase (sulfoglycosidase) from Prevotella strain RS2. *J. Bacteriol.* **2005**, *187*, 1543−1551.

https://dx.doi.org/10.1021/acs.langmuir.0c02256
Langmuir 2020, 36, 12973−12982

(61) Lottspeich, F.; Engels, J. W.; Solodkoff, Z. L. *Bioanalytik*; Spektrum Akademischer Verlag, 2012; pp 617−661.
(62) Chillappagari, S.; Preuss, J.; Licht, S.; Müller, C.; Mahavadi, P.; Sarode, G.; Vogelmeier, C.; Guenther, A.; Nahrlich, L.; Rubin, B. K. Altered protease and antiprotease balance during a COPD exacerbation contributes to mucus obstruction. *Respir. Res.* **2015**, *16*, 85.
(63) Hedstrom, L. Serine protease mechanism and specificity. *Chem. Rev.* **2002**, *102*, 4501−4524.

https://dx.doi.org/10.1021/acs.langmuir.0c02256
Langmuir 2020, 36, 12973−12982